ACS OMEGA

http://pubs.acs.org/journal/acsodf

Article

From Ta_2S_5 Wires to Ta_2O_5 and $Ta_2O_{5-x}S_x$

Shermane M. Benjamin,* Nathaniel F. Rieders, Michael G. Smith, and John J. Neumeier

Cite This: *ACS Omega* 2021, 6, 5445−5450

Read Online

ACCESS | Metrics & More | Article Recommendations | Supporting Information

ABSTRACT: Synthesis routes to forming novel materials are oftentimes complicated and indirect. For example, Ta_2S_5 has only been found as an unwanted byproduct of certain chemical reactions, and its properties were unknown. However, here we demonstrate the growth of Ta_2S_5 wires with steel-like tensile strength, which are also precursors for the first controlled synthesis of long, mesoscopic Ta_2O_5 wires and superconducting $Ta_2O_{5-x}S_x$ wires. Single-crystal wires of tantalum pentasulfide, Ta_2S_5, were first grown using vapor transport from polycrystalline XTa_2S_5, sulfur, and $TeCl_4$ in fused-quartz tubes, where X = Ba or Sr. Crystals form as long wires with lengths on the order of a few centimeters and varying cross sections as small as 25 μm^2. They were found to have steel-like tensile strength, and their crystal structure was determined using X-ray diffraction to be monoclinic with space group $P2/m$ and with lattice parameters a = 9.91(7) Å, b = 3.82(5) Å, and c = 20.92(2) Å. Electrical resistivity measurements reveal Ta_2S_5 to be a narrow band gap semiconductor with E_g = 110 meV, while a Debye temperature Θ_D = 97.0(5) K is observed in specific heat. Tantalum pentasulfide wires were then converted to insulating tantalum pentoxide (Ta_2O_5) wires after calcinating them for 30 min in air at 900 °C. Finally, tantalum pentoxide wires were converted to tantalum oxysulfide ($Ta_2O_{5-x}S_x$) wires after annealing them in CS_2 vapor for 30 min at 900 °C. The oxysulfide crystal structure was determined using X-ray diffraction to be that of β-Ta_2O_5. Electrical and magnetic measurements reveal $Ta_2O_{5-x}S_x$ to be metallic and superconducting with T_c = 3 K.

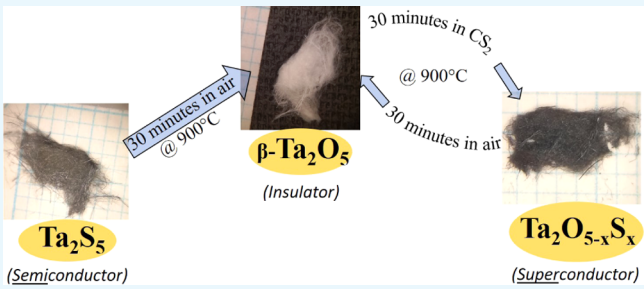

INTRODUCTION

The synthesis pathways to form advanced materials are not always direct. To date, Ta_2S_5 has only been reported as an unwanted nonmetallic inclusion in etched, pure tantalum[1,2] and as an unwanted byproduct[3] in thin-film production (e.g., CdS). Furthermore, there are no reports of the controlled formation of any single-crystalline binary tantalum chalcogenides with ratio 2:5 (e.g., Ta_2S_5, Ta_2Se_5, Ta_2Te_5, etc.). Regarding the oxide, for decades, tantalum pentoxide's (Ta_2O_5) tunable properties[4−7] have fortified its usefulness as an antireflective coating material, as a dielectric component for capacitors found in powered and powerless devices, and as a key material in photocatalysis.[8−10] Although Ta_2O_5 nanowires have high photocatalytic hydrogen evolution efficiencies attributed to their large surface-to-volume ratios and crystallinity,[9] to date, lengths beyond nanowires have not been realized but are highly desired.[8−10]

Similar to Ta_2O_5 nanowires, Ta_2O_5 nanocomposites with sulfur doped at 0.5 to 3.75 atomic % were shown to have enhanced photocatalytic efficiencies[11] when compared to the undoped. Enhanced efficiencies were, in part, due to improved crystallinity and increased surface area. In that example and many others,[12−14] sulfur-doped and undoped Ta_2O_5 were studied in their electrically insulating states because undoped Ta_2O_5 has a wide energy gap[15] of ∼4 eV.

In this report, we describe the first controlled synthesis of Ta_2S_5 wires with steel-like tensile strength. Afterward, we examine their role in the production of long mesoscopic wires of electrically insulating Ta_2O_5 and, in turn, metallic/superconducting mesoscopic wires of $Ta_2O_{5-x}S_x$. All wires were mesoscopic in thickness and macroscopic in length. Our results provide the synthesis routes for three compounds in wire form, consequently laying the experimental pathway for growing new inorganic, thin, long wires. The physical attributes of these compounds and their wire morphology offer potential for novel, practical applications.

RESULTS AND DISCUSSION

Properties of Ta_2S_5 Wires. For the synthesis of single-crystalline Ta_2S_5 wires (see Experimental Methods), polycrystalline XTa_2S_5 (X = Sr or Ba)[16,17] was first prepared. Our efforts to form Ta_2S_5 by heating Ta_2O_5 powder in CS_2 led only to bulk TaS_2 powder, and attempts to form Ta_2S_5 wires from Ta_2O_5 powder, sulfur, and $TeCl_4$ in a closed ampule were also not successful. The former attempt mirrored observations of previous investigators[18] and may suggest an inherent difficulty

Received: November 20, 2020
Accepted: February 3, 2021
Published: February 18, 2021

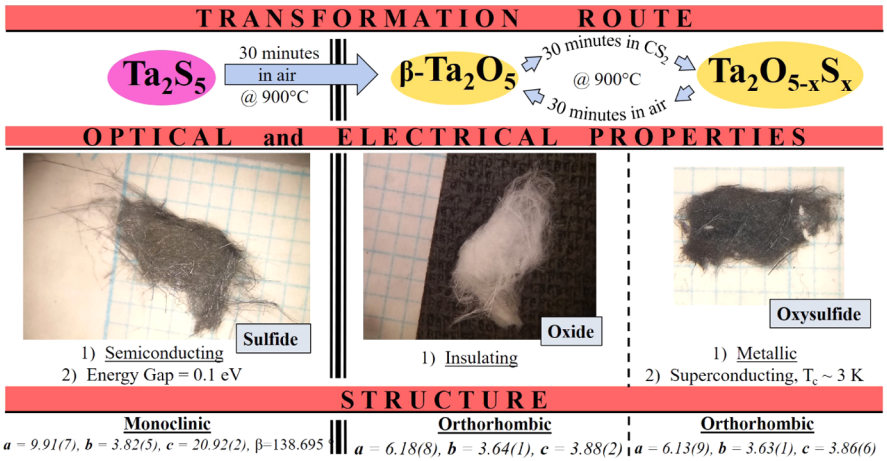

Figure 1. Tantalum wire conversions; a comparative data summary for wires of Ta_2S_5, Ta_2O_5, and $Ta_2O_{5-x}S_x$. Top row indicates the transformation route used to obtain Ta_2O_5 and $Ta_2O_{5-x}S_x$ from Ta_2S_5. Middle row depicts optical images and electrical properties of Ta_2S_5, Ta_2O_5, and $Ta_2O_{5-x}S_x$ from left to right. Squares within optical images represent 1 mm^2 footprints. Bottom row shows the indexed crystal structure and structure parameters for Ta_2S_5, Ta_2O_5, and $Ta_2O_{5-x}S_x$ from left to right. The figure can be expanded to view fine details in optical images.

in controlling the formation of bulk and therefore single-crystalline Ta_2S_5 from powder Ta_2O_5. The presence of other elements[19] may be required to drive the reaction toward Ta_2S_5 (e.g., strontium and barium used in our experiment) and may also clarify why controlled formation of Ta_2S_5 has eluded the materials community.

Ta_2S_5 wires are gray. Remarkably, their tensile strength is similar to steel at ∼1000 MPa (Figure S1 and Table S1). They are semiconducting with an approximate band gap of E_g = 110 meV, estimated from the linear fit of $\ln(\rho(T)/\rho(295\text{ K})) = E_g/2k_BT$ from the temperature region 48 K ≤ T ≤ 87 K. The variables $\rho(T)$, E_g, k_B, and T are the electrical resistivity, energy gap, Boltzmann constant, and temperature, respectively. Room-temperature electrical resistivity was estimated from a pelletized sample to be 1800 $\mu\Omega$ cm. Magnetic susceptibility measurements for 2 K to 296 K reveal Ta_2S_5 to be very weakly paramagnetic. Within a detection limit[20] of 0.1−0.3%, energy-dispersive X-ray spectroscopy (Figure S2) reveals the ratio of tantalum to sulfur at 2:5 (Table S2). Electron back-scattering diffraction (EBSD) patterns in Figure S2 show that the grown Ta_2S_5 wires are indeed single crystalline with the same crystallographic orientation along lengths of more than a few microns (see Figure S3 for indexing of Ta_2S_5's EBSD pattern). Ta_2S_5's powder diffraction pattern can be indexed to a monoclinic primitive cell (Figure 2c) with space group $P2/m$ and lattice parameters a = 9.91(7) Å, b = 3.82(5) Å, and c = 20.92(2) Å.

The specific heat C/T at constant pressure measured on tantalum pentasulfide over the temperature range 0.5 K < T < 10 K is shown in Figure 2g. Fitting the data to $C/T = \gamma T + \beta T^3$ within the depicted temperature range yielded the electron and phonon contributions to specific heat to be γ = 0.0073(2) mJ/mol K^2 and β = 0.0018(9) mJ/mol K^4, respectively. The Debye temperature, Θ_D, was calculated to be 97.0(5) K. The magnitude of Θ_D is comparable to transition-metal tantalum sulfides $BaTa_2S_5$ (Θ_D = 94 K[17]) and $SrTa_2S_5$ (Θ_D = 89.4 K[16]). Chen et al.[21] utilized the density functional theory plane-wave method to estimate the Debye temperature of β-Ta_2O_5 to be approximately 412 K.

Properties of Ta_2O_5 and $Ta_2O_{5-x}S_x$ Wires. Once Ta_2S_5 wires are available, Ta_2O_5 wires can be easily formed within 30 min by exposing them to air at 900 °C. This results in wires whose only optical difference from Ta_2S_5 is their white color. Ta_2O_5 is indexed to[22] orthorhombic β-Ta_2O_5. Thus, Ta_2S_5 and Ta_2O_5 differ in color and crystal structure but are shaped mesoscopically similar (Figures 1 and S4). Energy-dispersive X-ray spectra (EDS) data for Ta_2O_5 wires (Figure 2a) show that all sulfur is removed, within detection limits, during the evolution from Ta_2S_5 to Ta_2O_5. Powder X-ray diffraction shows Ta_2O_5 wires to be crystalline. Further measurements are needed to determine whether it is single crystalline or not.

After synthesizing Ta_2S_5 and Ta_2O_5 wires, one might ask if it is possible to reverse the reaction. Exploring the idea further, Ta_2O_5 wires were sulfurized in nitrogen gas laden with CS_2 for 30 min. Surprisingly, this led to the formation of $Ta_2O_{5-x}S_x$ wires that were black (Figure 1 and Figure S4). This process can be reversed by recalcinating $Ta_2O_{5-x}S_x$ in air for 30 min to recreate Ta_2O_5 wires. EDS data were taken on $Ta_2O_{5-x}S_x$ (Figure 2b) to compare to Ta_2O_5 (Figure 2a). It is clear from the data that sulfur is present in the former material but absent from the latter. Sulfur content, x, was estimated from the EDS spectra of $Ta_2O_{5-x}S_x$ to be ∼3.6 (±0.2), under the assumption that tantalum content is not altered during the reaction. In other words, approximately 75% of oxygen is replaced with sulfur. The accuracy of "x" was checked with large samples and a microbalance. However, with 8.5 mg (±0.5 mg) of Ta_2O_5 converted to 9.2 mg (±0.5 mg) of $Ta_2O_{5-x}S_x$, we see x = 2.2 (±0.7). We believe that the discrepancy between the value derived from the microbalance and the one calculated from EDS (x = 3.6) is due to an error in the weighing methodology. Improved calculations are possible with even larger samples; however, it is not currently feasible since our synthesis pathway produces low yields.

Similar to Ta_2O_5 wires, X-ray diffraction reveals $Ta_2O_{5-x}S_x$ wires to be crystalline, but further measurements are required to determine if it is also single crystalline. Tantalum oxysulfide, $Ta_2O_{5-x}S_x$, was indexed to the same orthorhombic structure and lattice parameters as Ta_2O_5, within uncertainties (Figure 2c). This means Ta_2O_5 and $Ta_2O_{5-x}S_x$ are structurally indistinguishable.

The formation of oxysulfide wires from Ta_2O_5 wires is quite surprising since TaS_2 is the expected product after the reaction of Ta_2O_5 powder with CS_2 or H_2S.[18] Our results reveal that Ta_2O_5 in wire form seems to accept substitutions of sulfur from

https://dx.doi.org/10.1021/acsomega.0c05656
ACS Omega 2021, 6, 5445−5450

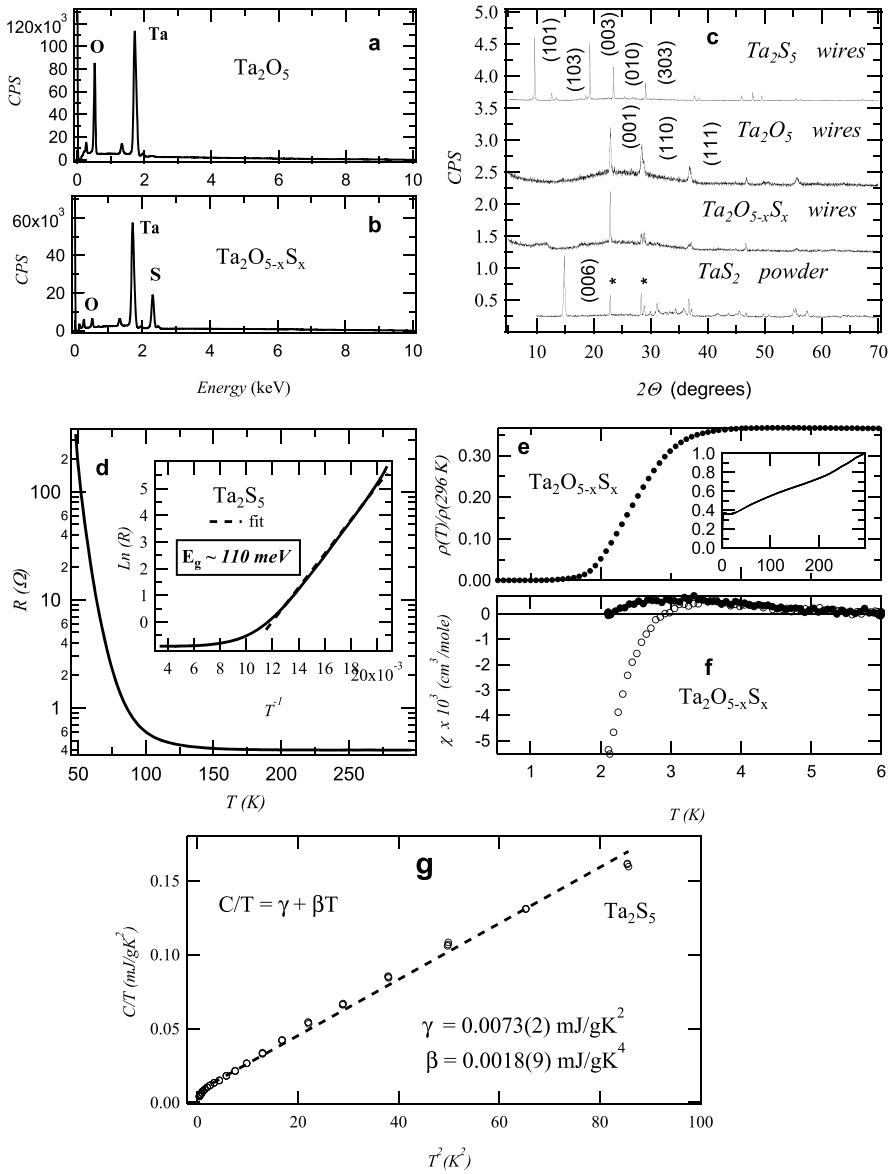

Figure 2. Properties of Ta_2S_5, Ta_2O_5, and $Ta_2O_{5-x}S_x$ wires. (a) EDS obtained from Ta_2O_5 and oxysulfide (b) $Ta_2O_{5-x}S_x$ where $x \sim 3.6$. (c) X-ray diffraction scans of Ta_2S_5, Ta_2O_5, $Ta_2O_{5-x}S_x$, and TaS_2 obtained with Cu Kα radiation. X-ray scans for Ta_2O_5 and $Ta_2O_{5-x}S_x$ were indexed to[22] orthorhombic β-Ta_2O_5. The X-ray pattern for TaS_2 can be indexed to[23] rhombohedral 3R-TaS_2, where asterisks depict unreacted Ta_2O_5. (d) Temperature-dependent electrical resistance of pelletized Ta_2S_5. An energy gap, E_g, was found to be approximately 110 meV from the temperature region 48 K $\leq T \leq$ 87 K. (e) Normalized resistance versus temperature of pelletized $Ta_2O_{5-x}S_x$ within the superconducting region at low temperature below 6 K where $T_{c\text{-onset}} \sim 3$ K. The inset displays the entire metallic region of resistance for $Ta_2O_{5-x}S_x$. (f) Magnetic susceptibility χ of pelletized $Ta_2O_{5-x}S_x$ with width = 3 mm, length = 5 mm, and thickness = 0.5 mm. χ data (open symbols) obtained after cooling the sample in zero magnetic field to 2.1 K, followed by application of the magnetic field H = 38 Oe and warming of the sample during the measurement; this is the shielding curve. The solid symbols were obtained by cooling from 6 K in H = 38 Oe; this is the Meissner curve. (g) Specific heat capacity C/T vs T^2 of pelletized Ta_2S_5 below 10 K. The Debye temperature, Θ_D, derived from the plot is 97.(5) K.

CS_2 for oxygen without undergoing a structural change to the 3R-TaS_2 rhombohedral structure,[23] as one would expect.

The physical properties of tantalum oxysulfide are equally surprising. As the temperature decreases, its electrical resistance is metallic, dropping to approximately 40% of the room-temperature value before the onset of superconductivity at $T_c \sim$ 3 K. The electrical resistance is essentially zero at $T \leq 1$ K. Meissner and shielding volume fractions at T = 2.1 K, the low-temperature limit of our equipment, revealed by magnetic susceptibility measurements were 0.58 and 5.2%, respectively, as shown in Figure 2f. Note that it is not uncommon to observe small Meissner fractions in sulfides despite bulk superconductivity.[16,17] Thus, a narrow band gap semiconductor (Ta_2S_5) is oxidized to form an insulator (Ta_2O_5) that is sulfurized to form a metallic superconductor ($Ta_2O_{5-x}S_x$), all while maintaining the morphology of mesoscopic wires.

DISCUSSION

The electronegativity and size of oxygen and sulfur likely dictate the dynamics and outcome of the following reactions: $Ta_2S_5 \rightarrow Ta_2O_5$ and $Ta_2O_5 \rightarrow Ta_2O_{5-x}S_x$. The former reaction completely replaces sulfur for oxygen probably because oxygen's ionic volume is 2.25 times smaller than sulfur's and is more electronegative.[24] However, the latter transformation demands a

https://dx.doi.org/10.1021/acsomega.0c05656
ACS Omega 2021, 6, 5445−5450

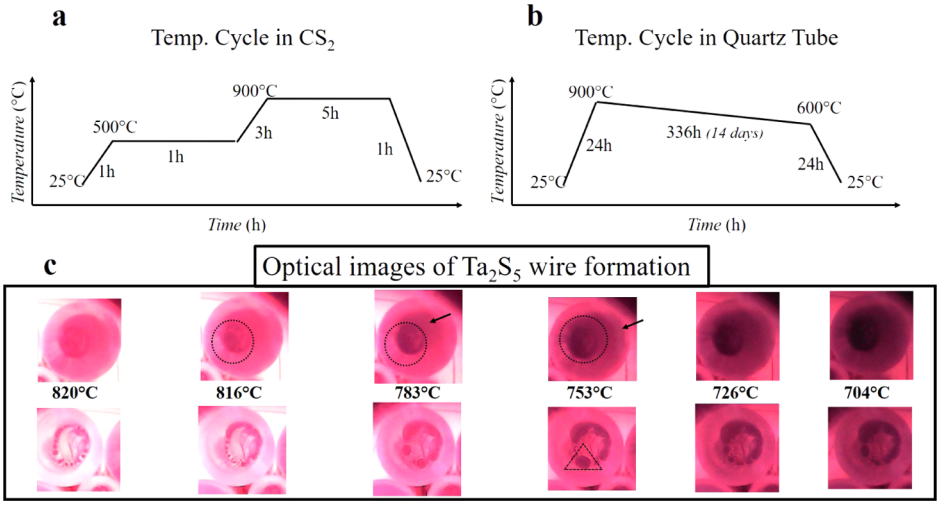

Figure 3. Synthesis temperature cycles for Ta_2S_5. (a) Temperature cycle of contents placed in the hottest zone of the CS_2 tube furnace. (b) Temperature cycle of mixture in a sealed quartz tube placed in a tube furnace. (c) Optical images of Ta_2S_5 wire growth attempts in sealed quartz tubes as temperature slowly decreases. Images are views of the coldest end of two sealed quartz tubes, parallel to the long axis of each tube, in a heated furnace. Top row indicates Ta_2S_5 wire growth, while the bottom row shows attempts to grow Ta_2S_5 wires in the presence of water. Dotted circles enclose the formation of a sulfur-rich surface which grows first at around 816 °C, as indicated by the darkened center region. Ta_2S_5 sprouts from this surface as shown by the arrow at 783 °C. Below 783 °C, Ta_2S_5 continues to grow as indicated by the "cloudy" region surrounding the center dotted circle that remains unchanged. In the presence of water, however, something forms at around 753 °C, as indicated by the dotted triangle and then disappears as the temperature decreases. Quartz tubes with water yielded no Ta_2S_5 wires.

larger atom (sulfur) that is also less electronegative to replace oxygen, leading to an incomplete substitution under similar synthesis conditions. The existence of a simple compound such as Ta_2S_5 that can easily transform to other compounds (Ta_2O_5 and $Ta_2O_{5-x}S_x$) while maintaining the structural morphology is unusual, and the fact that each of the three reported compounds has widely varying electronic properties adds to the novelty of this work.

Superconductivity in oxysulfides is exceedingly rare.[25] Since the first reported bulk bismuth oxysulfide superconductor, $Bi_4O_4S_3$[26] [T_c = 4.4 K], only bismuth-based, BiS-layered oxysulfide compounds have been reported.[27] These include[28] $LaOBiS_2$ [T_c = 3.6 K] and[27] $La_{1.7}Eu_{0.3}O_2Bi_3Ag_{0.6}Sn_{0.4}S_6$ [T_c = 3.64 K], which have between four and seven elements. Therefore, $Bi_4O_4S_3$ and $Ta_2O_{5-x}S_x$ can be considered "simple oxysulfides," as they are composed of only three elements each. Thus, $Ta_2O_{5-x}S_x$ is one of the few known oxysulfide superconductors and the first simple transition-metal oxysulfide superconductor containing only a transition metal, oxygen, and sulfur.

The discovery of superconductivity in $Ta_2O_{5-x}S_x$ makes it and $Bi_4O_4S_3$ the only known superconducting ternary oxysulfides.[25] Bismuth oxysulfide has BiS layers that are presumed to play a role in superconductivity, like CuO layers do in high-temperature superconducting cuprates.[29] Further work is needed to determine the atomic arrangement for $Ta_2O_{5-x}S_x$ and, most importantly, the nature of its superconductivity. Large single crystal $Ta_2O_{5-x}S_x$ samples are needed to elucidate the above matters.

The tensile strength of the Ta_2O_5 and $Ta_2O_{5-x}S_x$ wires could not be quantified within the limits of our measurement apparatus because they were soft and brittle. Careful micromanipulation of these phases could not be achieved because they lacked physical strength. However, due to the flexibility and steel-like tensile strength of Ta_2S_5, many physical shapes of Ta_2O_5 and $Ta_2O_{5-x}S_x$ wires are obtainable after oxidizing Ta_2S_5 wires and sulfurizing its products. Therefore, physical manipulation of all wires to form specific geometries is possible, which might enable the formation of uniquely shaped single-photon detectors[30] or superconducting loops for SQUID sensors in quantum device applications.

Although our synthesis process (Figure 3) is reproducible and completely bypasses forming the bulk phases of the sulfide, oxide, and oxysulfide compounds, it is grossly inefficient. During the synthesis of Ta_2S_5 wires, less than ∼0.1% of the starting mass (CS_2 + Ta_2O_5 + $SrCO_3$ or $BaCO_3$ + $TeCl_4$) is converted to wires. Oxygen, tellurium, carbon, and barium or strontium are considered waste elements in this context. However, as previously indicated, such mass inefficiencies may be necessary to form the elusive Ta_2S_5 phase.

Finally, the nearly cyclical relationship among the synthesis of Ta_2S_5, Ta_2O_5, and $Ta_2O_{5-x}S_x$ wires might suggest a possible route to create crystalline Ta_2Se_5 wires. Se^{2-}'s electronegativity[31] is approximately 2% less than S^{2-}, and its ionic volume is 2.8 times larger than oxygen's, as opposed to S^{2-} being 2.4 times larger than oxygen.[24] These factors may be adequate to allow formation of Ta_2Se_5 by exposing Ta_2S_5 (or Ta_2O_5) to a selenium-rich atmosphere at elevated temperatures. On the other hand, our synthesis results suggest that Ta_2Te_5 may be difficult, if not impossible, to form. Tellurium was not detected in our Ta_2S_5 wires, within EDS detection limits, although it was a component of the chemical vapor transport agent. This may be because tellurium's electronegativity[31] is nearly 20% less than sulfur's, and its ionic volume is 3.93 times larger than oxygen's,[24] thus hindering the growth of the oxytelluride phase, $Ta_2O_{5-x}Te_x$. Tantalum sulfide's (Ta_2S_5) energy gap is 110 meV, around 500 times less than tantalum oxide's (Ta_2O_5) energy gap.[15] If tantalum selenide (Ta_2Se_5) exists, its gap might be smaller, or may even vanish, possibly giving rise to another new conducting wire with novel physical properties.

■ CONCLUSIONS

Single-crystal Ta_2S_5 wires reveal narrow band gap semiconducting behavior below 296 K with energy gap E_g = 110

https://dx.doi.org/10.1021/acsomega.0c05656
ACS Omega 2021, 6, 5445−5450

meV. Ta_2S_5's unit cell is indexed to a monoclinic structure whose space group is most likely $P2/m$. High-temperature calcination of Ta_2S_5 wires converts them to insulating Ta_2O_5 wires. High-temperature sulfurization of Ta_2O_5 wires leads to metallic, superconducting $Ta_2O_{5-x}S_x$ wires.

■ EXPERIMENTAL METHODS

To make single-crystalline Ta_2S_5 wires, polycrystalline XTa_2S_5 (X = Sr or Ba) was first synthesized. The initial mixture of stoichiometric carbonates $SrCO_3$ or $BaCO_3$ and commercially available powdered Ta_2O_5 was transferred to an alumina crucible, which was placed in a tube furnace at room temperature. Nitrogen gas was passed through an aeration stone immersed in CS_2 and then through the tube furnace. The tube furnace was contained in a fume hood to exhaust CS_2 fumes from the laboratory. The following temperature cycle was initiated (Figure 3a). It was ramped to 500 °C over an hour where it remained for an hour, then ramped to 900 °C over a 3 h period where it remained for another 5 h. Finally, the sample was cooled to room temperature over a 1 h period. The sample was then placed in an evacuated sealed quartz tube with sulfur at 2% of its weight and $TeCl_4$, which naturally produces chlorine gas in the tube. The chlorine gas only served as a transport agent during synthesis, and Te and Cl were absent from the wires. Just enough $TeCl_4$ was added to create approximately 1 atm of pressure at 900 °C; the required mass was calculated from the dimensions of the quartz tube and the ideal gas law $PV_{tube} = nRT$. P, V_{tube}, n, R, and T are the pressure (e.g., 1 atm), tube volume, number of moles, gas constant, and temperature (e.g., 900 °C), respectively. The quartz tube was then placed in a single-zone tube furnace. For this cycle (Figure 3b), contents within the tube were placed at one end (i.e., left side) of the tube, located at the hottest spot in the oven, which was subsequently ramped to 900 °C over a 24 h period. The left side where the mixture was located in our experiment was centered at the hottest spot of the oven. The opposing end of the tube (i.e., right side) was approximately 19 cm away at a constant temperature difference of 80 °C below the left side because of its distance from the furnace's hottest spot. The mixture (i.e., left side) was then slow cooled to 600 °C over 14 days. Finally, the quartz tube was cooled to room temperature over a 24 h period. This process yielded gray-colored Ta_2S_5 wires on the right side of the tube. Optical analysis of the radiated infrared light emitted from the cold side during the second temperature cycle suggests that Ta_2S_5 wires grow below 783 °C (Figure 3c).

Three important things to note for successfully growing Ta_2S_5 wires are the presence of tellurium chloride ($TeCl_4$), the effects of temperature gradients, and slow cooling, as shown in Figure 3b. Wires did not form when $TeCl_4$ was removed or exchanged for water as a transport agent. They also did not form if the temperature was held at 900 °C for 14 days, as opposed to slow cooling between 900 and 600 °C for 14 days.

Tantalum pentasulfide wires are transformed into Ta_2O_5 and $Ta_2O_{5-x}S_x$ wires in the following manner. First, Ta_2O_5 wires are formed after calcinating Ta_2S_5 wires for 30 min in air at 900 °C, after ramping to 900 °C within 20 min. Second, $Ta_2O_{5-x}S_x$ wires are formed after heating Ta_2O_5 wires in CS_2 for 30 min at 900 °C, after ramping to 900 °C within 20−30 min. The latter process is reversible, so one can recreate Ta_2O_5 wires from $Ta_2O_{5-x}S_x$ wires by calcinating the oxysulfide in air for 30 min at 900 °C, after ramping to 900 °C within 20 min. Cooling rates to acquire Ta_2O_5 and $Ta_2O_{5-x}S_x$ may affect surface roughness but are independent of their formation within the tested parameters.

It must be noted that using Ta_2O_5 powder does not yield similar results; only Ta_2O_5 wires produce $Ta_2O_{5-x}S_x$ wires when reacted with CS_2. Powdered Ta_2O_5 reacting with CS_2 at 900 °C yields TaS_2 powder (Figure 2c).[18]

For stoichiometry and structural phase identification, EDS and powder X-ray diffraction data were collected on finely crushed wires of Ta_2S_5, Ta_2O_5, and $Ta_2O_{5-x}S_x$. EDS spectra were acquired in a custom-built PHI 710 integrated scanning Auger nanoprobe (Physical Electronics; Chanhassen, MN, USA). A 20 keV electron beam was used to generate X-rays, which were collected by a silicon drift detector (Bruker XFlash; Billerica, MA). Quantification of EDS spectra was performed using a ZAF model.[20]

For EBSD data, a 20 keV beam was used with the sample tilted to 70° from the horizontal (i.e., electrons entered the surface at a ∼20° grazing angle). The resulting EBSD patterns were recorded on a phosphorus screen coupled to a CCD camera (ThorLabs 1500M-GE-EX1; Newton, NJ). Electrical and magnetic measurements were carried out with a Quantum Design Physical Properties Measurement System. Ta_2S_5's electrical resistance was measured with a four-probe dc method on a pelletized sample of length 0.92(5) mm and cross-sectional area 0.052(6) mm^2. Current densities of around 190 mA/cm^2 were utilized to avoid Joule resistive heating. The uncertainty in electrical resistivity is about 5% due to geometrical errors. Temperature-dependent resistance measurements were done on $Ta_2O_{5-x}S_x$. Ta_2S_5 wires were pelletized for all measurements except X-ray diffraction. A PASCO wireless force acceleration sensor was used to measure Ta_2S_5's tensile strength. See Figure S1 and Table S1 for tensile strength measurement details.

■ ASSOCIATED CONTENT

Supporting Information

The Supporting Information is available free of charge at https://pubs.acs.org/doi/10.1021/acsomega.0c05656.

Tensile strength measurement setup and results for Ta_2S_5 wires, EBSD pattern and quantified energy-dispersive X-ray results for Ta_2S_5 wires, and scanning electron microscope images of all three compounds (PDF)

■ AUTHOR INFORMATION

Corresponding Author

Shermane M. Benjamin − *Physics Department, Montana State University, Bozeman, Montana 59717-3840, United States;* orcid.org/0000-0003-0594-7490; Email: sbenjamin21@gmail.com

Authors

Nathaniel F. Rieders − *Physics Department, Montana State University, Bozeman, Montana 59717-3840, United States*

Michael G. Smith − *Physics Department, Montana State University, Bozeman, Montana 59717-3840, United States*

John J. Neumeier − *Physics Department, Montana State University, Bozeman, Montana 59717-3840, United States*

Complete contact information is available at: https://pubs.acs.org/10.1021/acsomega.0c05656

Author Contributions

Scientific ideas and concepts were the results of discussions and interactions among all authors. S.M.B. and N.F.R. conducted the electron microscopy experiments and subsequent data analysis. S.M.B. synthesized all specimens and conducted tensile stress

https://dx.doi.org/10.1021/acsomega.0c05656
ACS Omega 2021, 6, 5445−5450

measurements and electric and magnetic property measurements and the data analysis which followed. All authors cowrote and edited the manuscript.

Funding

Work at Montana State University was conducted with financial support from the US Department of Energy (DOE), Office of Science, Basic Energy Sciences (BES) under award no. DE-SC0016156; this includes the growth, characterization, physical property measurements, and data analysis, which were conducted by S.M.B., N.F.R., M.G.S., and J.J.N. S.M.B acknowledges additional financial support from MSU's College of Letters and Science. Electron microanalysis and X-ray powder diffraction measurements were performed at the Montana Nanotechnology Facility, a member of the National Nanotechnology Coordinated Infrastructure (NNCI), which is supported by the National Science Foundation grant no. ECCS-1542210.

Notes

The authors declare no competing financial interest.

■ ACKNOWLEDGMENTS

We thank N. J. Borys for useful discussions.

■ REFERENCES

(1) de Haas, W. J.; Capel, W. H. The thermal resistance of bismuth single-crystals at low temperatures. *Physica* **1934**, *1*, 929−934.

(2) Gale, W. F.; Totemeier, T. C. *Smithells Metals Reference Book*; Elsevier, 2003.

(3) Cardon, F. *Photovoltaic and Photoelectrochemical Solar Energy Conversion*; Springer Science & Business Media, 2012.

(4) Bright, T. J.; Watjen, J. I.; Zhang, Z. M.; Muratore, C.; Voevodin, A. A.; Koukis, D. I.; Tanner, D. B.; Arenas, D. J. Infrared optical properties of amorphous and nanocrystalline Ta_2O_5 thin films. *J. Appl. Phys.* **2013**, *114*, 083515.

(5) Porqueras, I.; Marti, J.; Bertran, E. Optical and electrical characterisation of Ta_2O_5 thin films for ionic conduction applications. *Thin Solid Films* **1999**, *343*−*344*, 449−452.

(6) Markosyan, A. S.; Route, R.; Fejer, M. M.; Patel, D.; Menoni, C. Study of spontaneous and induced absorption in amorphous Ta_2O_5 and SiO_2 dielectric thin films. *J. Appl. Phys.* **2013**, *113*, 133104.

(7) Shibata, S. Dielectric constants of Ta_2O_5 thin films deposited by r.f. sputtering. *Thin Solid Films* **1996**, *277*, 1−4.

(8) Cheng, S.; Sang, L.; Liao, M.; Liu, J.; Imura, M.; Li, H.; Koide, Y. Integration of high-dielectric constant Ta_2O_5 oxides on diamond for power devices. *Appl. Phys. Lett.* **2012**, *101*, 232907.

(9) Lü, X.; Ding, S.; Lin, T.; Mou, X.; Hong, Z.; Huang, F. Ta_2O_5 nanowires: a novel synthetic method and their solar energy utilization. *Dalton Trans.* **2012**, *41*, 622−627.

(10) Chapman, R.; Monaldo, F. M. A Novel Wave Height Sensor. *J. Atmos. Ocean. Technol.* **1995**, *12*, 190−196.

(11) Ismail, A. A.; Faisal, M.; Harraz, F. A.; Al-Hajry, A.; Al-Sehemi, A. G. Synthesis of mesoporous sulfur-doped Ta_2O_5 nanocomposites and their photocatalytic activities. *J. Colloid Interface Sci.* **2016**, *471*, 145−154.

(12) Moon, B. K.; Isobe, C.; Aoyama, J. Insulating properties of tantalum pentoxide capacitor films obtained by annealing in dry ozone. *J. Appl. Phys.* **1999**, *85*, 1731−1738.

(13) Sedghi, N.; Li, H.; Brunell, I. F.; Dawson, K.; Guo, Y.; Potter, R. J.; Gibbon, J. T.; Dhanak, V. R.; Zhang, W. D.; Zhang, J. F.; Hall, S.; Robertson, J.; Chalker, P. R. Enhanced switching stability in Ta_2O_5 resistive RAM by fluorine doping. *Appl. Phys. Lett.* **2017**, *111*, 092904.

(14) Webb, A. G. Dielectric materials in magnetic resonance. *Concepts Magn. Reson., Part A* **2011**, *38A*, 148−184.

(15) Chun, W.-J.; Ishikawa, A.; Fujisawa, H.; Takata, T.; Kondo, J. N.; Hara, M.; Kawai, M.; Matsumoto, Y.; Domen, K. Conduction and Valence Band Positions of Ta_2O_5, TaON, and Ta_3N_5 by UPS and Electrochemical Methods. *J. Phys. Chem. B* **2003**, *107*, 1798−1803.

(16) Drenner, A. K.; Benjamin, S. M.; Smith, M. G.; Neumeier, J. J. Physical properties and superconductivity of $SrTa_2S_5$. *Phys. C* **2019**, *556*, 19−23.

(17) Drenner, A. K.; Benjamin, S. M.; Smith, M. G.; Neumeier, J. J. Physical properties and superconductivity of $BaTa_2S_5$. *Phys. C* **2019**, *566*, 1353522.

(18) Schmidt, F. F. *Tantalum and Tantalum Alloys: Report*; Defense Metals Information Center, 1960.

(19) Sarazin, Y.; Carpentier, J.-F. Calcium, Strontium and Barium Homogeneous Catalysts for Fine Chemicals Synthesis. *Chem. Rec.* **2016**, *16*, 2482−2505.

(20) Goldstein, J.; Newbury, D.; Joy, D.; Lyman, C. *Scanning Electron Microscopy and X-ray Microanalysis*, 3rd ed.; Kluwer Academic 1 Plenum Publishers: New York, 2003.

(21) Chen, Z.; Hu, M.; Li, C.; Li, F. Electronic structures, elastic and optical properties of M2O5 (M = V, Nb, Ta). *Sci. China Mater.* **2016**, *59*, 265−278.

(22) Lehovec, K. Lattice structure of β-Ta_2O_5. *J. Less-Common Met.* **1964**, *7*, 397−410.

(23) Haegg, G.; Schoenberg, N. X-ray studies of sulfides of titanium, zirconium, niobium, and tantalum. *Ark. Kemi* **1954**, *7*, 371−380.

(24) Shannon, R. D. Revised effective ionic radii and systematic studies of interatomic distances in halides and chalcogenides. *Acta Crystallogr., Sect. A: Cryst. Phys., Diffr., Theor. Gen. Crystallogr.* **1976**, *32*, 751−767.

(25) Larquet, C.; Carenco, S. Metal Oxysulfides: From Bulk Compounds to Nanomaterials. *Front. Chem.* **2020**, *8*, 179.

(26) Singh, S. K.; Kumar, A.; Gahtori, B.; Shruti; Sharma, G.; Patnaik, S.; Awana, V. P. S. Bulk Superconductivity in Bismuth Oxysulfide $Bi_4O_4S_3$. *J. Am. Chem. Soc.* **2012**, *134*, 16504−16507.

(27) Jha, R.; Mizuguchi, Y. Superconductivity in $La_2O_2M_4S_6$ -Type Bi-based Compounds: A Review on Element Substitution Effects. *Condens. Matter* **2020**, *5*, 27.

(28) Uesugi, E.; Nishiyama, S.; Goto, H.; Ota, H.; Kubozono, Y. Electrostatic electron- doping yields superconductivity in $LaOBiS_2$. *Appl. Phys. Lett.* **2016**, *109*, 252601.

(29) Mizuguchi, Y.; Fujihisa, H.; Gotoh, Y.; Suzuki, K.; Usui, H.; Kuroki, K.; Demura, S.; Takano, Y.; Izawa, H.; Miura, O. Novel BiS_2-based layered superconductor $Bi_4O_4S_3$. *Phys. Rev. B: Condens. Matter Mater. Phys.* **2012**, *86*, 220510.

(30) Korzh, B.; et al. Demonstration of sub-3 ps temporal resolution with a superconducting nanowire single-photon detector. *Nat. Photonics* **2020**, *14*, 250−255.

(31) Murphy, L. R.; Meek, T. L.; Allred, A. L.; Allen, L. C. Evaluation and Test of Pauling's Electronegativity Scale. *J. Phys. Chem. A* **2000**, *104*, 5867−5871.

https://dx.doi.org/10.1021/acsomega.0c05656
ACS Omega 2021, 6, 5445−5450